CRISPR/Cas9-mediated Genomic Editing of Cluap1/IFT38 Reveals a New Role in Actin Arrangement*[S]

Tina Beyer‡, Sylvia Bolz‡, Katrin Junger‡, Nicola Horn‡, Muhammad Moniruzzaman‡, Yasmin Wissinger‡§, Marius Ueffing‡¶, and Karsten Boldt‡¶

CRISPR/Cas9-mediated gene editing allows manipulation of a gene of interest in its own chromosomal context. When applied to the analysis of protein interactions and in contrast to exogenous expression of a protein, this can be studied maintaining physiological stoichiometry, topology, and context. We have used CRISPR/Cas9-mediated genomic editing to investigate Cluap1/IFT38, a component of the intraflagellar transport complex B (IFT-B). Cluap1 has been implicated in human development as well as in cancer progression. Cluap1 loss of function results in early developmental defects with neural tube closure, sonic hedgehog signaling and left–right defects. Herein, we generated an endogenously tagged Cluap1 for protein complex analysis, which was then correlated to the corresponding interactome determined by ectopic expression. Besides IFT-B complex components, new interacting proteins like Ephrin-B1 and TRIP6, which are known to be involved in cytoskeletal arrangement and protein transport, were identified. With the identification of platelet-derived growth factor A (PDGFA) and coiled-coil domain-containing protein 6 (CCDC6) two new interactions were discovered, which link Cluap1 to ciliogenesis and cancer development. The CRISPR/Cas9-mediated knockout of Cluap1 revealed a new phenotype affecting the actin cytoskeleton. Together, these data provide first evidence for a role of Cluap1 not only for cilia assembly and maintenance but also for cytoskeletal rearrangement and intracellular transport processes. ***Molecular & Cellular Proteomics 17: 10.1074/mcp.RA117.000487, 1285–1294, 2018.***

Before the first demonstration of clustered regularly interspaced short palindromic repeats (CRISPR)/Cas9[1]-mediated gene editing in 2013 (1, 2), analysis of gene function has largely been dependent on exogenous gene expression. This has produced an enormous amount of information yet always compromised by the fact that exogenous gene expression would perturb the endophenotype of a cell and thereby produce artifacts (3). We decided to employ CRISPR/Cas9-mediated gene editing to study protein interactions at endogenous levels to specifically target a protein of interest, clusterin-associated protein 1 (Cluap1), a protein found in vertebrate cilia. Cilia are protrusions of the cell and are involved in multiple cell- and tissue-related processes. Motile cilia are necessary for the motion of extracellular fluids, including signaling components packed in vesicles or clearance of pathogens and dirt, for instance. Nonmotile or primary cilia mainly serve as sensory organelles and center for the transduction of extracellular signaling events, which could be either a mechanical force, *e.g.* the kinocilium in the inner ear, or specific pathway activation through ligand–receptor binding, as it is shown for sonic hedgehog or platelet-derived growth factor receptor signaling. A specialized cilia type is represented by the connecting cilium of the photoreceptor, which is essential for protein exchange between the outer and the inner segment (4–6).

Failure of cilia assembly or cilia-dependent signaling processes can lead to a variety of diseases, which are summarized as ciliopathies. Depending on the underlying mutation, the phenotype can range from isolated defects, such as retinal degeneration, cystic kidney and pancreas, to syndromic forms, which may include polydactyly, obesity, and heart failure. In most cases, a complete loss of a structural cilia protein result in early developmental deficiencies, including hydrocephalus, neural tube closure, and left–right defects (7, 8).

The basic components of any cilium are the basal body structure with a modified mother and daughter centriole and the central axoneme, which is built out of nine microtubule doublets. The axoneme is maintained by a permanent transport and turnover of tubulin from the ciliary base to the tip and vice versa (9). Motor proteins conduct the transport of proteins with kinesins being involved in the anterograde and dyneins being necessary for the retrograde transport of cargo. Kinesins interact with IFT-B protein complexes, which are

From the ‡Institute for Ophthalmic Research, Centre for Ophthalmology, University of Tübingen, Elfriede-Aulhorn-Strasse 7, D-72076 Tübingen, Germany; §Thermo Fisher Scientific, Clinical Diagnostics Systems, Neuendorfstr. 25, 16761 Hennigsdorf, Germany

Received December 5, 2017, and in revised form, March 28, 2018
Published, MCP Papers in Press, April 3, 2018, DOI 10.1074/mcp.RA117.000487

necessary for cargo binding and selective transport into the cilium and along the axoneme. Dyneins attach to the IFT-A complex for transport of signaling molecules and cilia structure proteins out of the cilium. Cilium assembly is not affected in IFT-A-related diseases, but IFT-B mutations often result in shortened or lost cilia (10, 11). Besides their role in cilia assembly and maintenance, there are some evidences for IFT-B protein function in cell cycle regulation, migration, cytoskeletal arrangement, and protein transport in the cytoplasm. For example, the IFT-B proteins IFT20, IFT88, IFT57, and IFT54/TRAF3IP1 are shown to be jointly involved in T cell antigen receptor localization and recycling in immune synapses of Jurkat T cells (12). In addition, in 2015, Bizet and colleagues showed that IFT54/TRAF3-interacting protein 1 (TRAF3IP1) regulates cytoplasmic microtubule stability and cell polarity via microtubule-associated protein 4 (MAP4) modulation (13). IFT88 was described to be involved in organizing microtubules at the leading edge in migrating cells and to be necessary for polarized cell division (14–16).

Cluap1/IFT38 is shown to be part of the IFT subcomplex B2 and is able to form homodimers or heterodimers with IFT57 (17, 18). The IFT57/IFT38 seems to be the linker to the IFT-B1 complex through interaction with IFT88/IFT52 and the other IFT-B2 complex components. A complete loss of Cluap1 in mice results in embryonic lethality caused by typical ciliary defects, confirming the central role of Cluap1 (19, 20). Cluap1/qilin truncation in zebrafish larvae leads to cystic kidneys, curved bodies, and photoreceptor degeneration (21). Recently, a hypomorphic mutation in the coiled-coil domain of Cluap1 was described that led to the specific phenotype of early-onset retinal degeneration called Leber congenital amaurosis (LCA, 22). Interestingly, besides the role of Cluap1 in ciliopathic diseases, Cluap1 expression is shown to be upregulated in colon cancer in a cell-cycle dependent manner (23).

The different functions one single protein can have depend on posttranslational modification, localization, and protein complex formation, for instance. To determine functional relevant interactions, affinity purification of protein complexes is used. But often, massive overexpression of single isoforms of the protein of interest is performed to produce tagged protein in cell culture that might lead to artificial results due to protein misfolding, high nonregulated protein level imbalance and cell toxicity (3). Recently, insertion of small tag coding sequences into specific regions of the genome was used to avoid these problems (24, 25).

Applying such CRISPR/Cas9-mediated gene editing in combination with mass spectrometric analysis, new protein interactions of Cluap1 could be described using two different approaches: 1) CRISPR/Cas9-mediated endogenous FLAG-tag insertion into the Cluap1 gene to avoid artificial results often seen in overexpression datasets and 2) overexpression of three different isoforms followed by comparative analysis using quantitative mass spectrometry (Fig. 1). Both approaches revealed new Cluap1 complex components outside the well-known IFT-B2 subcomplex. We were able to describe new Cluap1 interactors that have previously been described as ciliary, such as BBSome proteins. Further, we could identify novel protein interactions involved in cytoskeletal arrangement. This links Cluap1 to both, ciliary-IFT-driven transport as well as cytoskeletal dynamics opening the possibility that these two physiological activities are interlinked as well.

EXPERIMENTAL PROCEDURES

Cloning of CRISPR/Cas9 Constructs—For knockout (KO) and knock-in experiments the pSpCas9(BB)-2A-Puro (PX459) V2.0 was used (gift from Feng Zhang (Addgene plasmid # 62988)). The sgRNA was cloned as described elsewhere (26). Briefly, sgRNA top and bottom oligos were phosphorylated and aligned. The pSpCas9(BB)-2A-Puro vector was cut using the Bbs1 restriction enzyme and ligated with the sticky end harboring double-stranded sgRNA. The final construct was transformed into DHC5α^{TM} (Invitrogen^{TM}) and bacteria were grown under ampicillin selection. DNA was isolated using a PureYield^{TM} Plasmid Midi Preparation Kit (Promega).

Generation of Knockout/Knock-in hTERT-RPE-1 and HEK293T Cell Lines—HTERT-RPE-1 and HEK293T cells were grown in DMEM supplemented with 10% fetal bovine serum (FBS) and 0.5% penicillin/streptomycin at 37 °C in 5% CO_2. HTERT-RPE-1 cells were transfected using lipofectamine 2000 or 3000 (Invitrogen), HEK293T using homemade polyethylenimine solution. As control, cells were transfected with the pSpCas9(BB)-2A-Puro vector harboring no gene-targeting sgRNA. 48 h posttransfection, cells were transferred into puromycin-containing medium (Thermo Fisher Scientific, HEK293T 3 μg/ml for 3 days, hTERT-RPE-1 40 μg/ml for 5 days). Living cells were transferred in low concentration to a 14-cm plate for single clone selection and single colonies were pipetted to a 12-well plate 2–3 days later. For sequencing the genomic region, DNA was isolated using peqGold tissue DNA Mini Kit (VWR), the region of interest was amplified, and the PCR product was purified using the CyclePure Kit (VWR) and sent for sequencing (GATC, Germany).

Protein Complex Analysis by FLAG- or Streptavidin-Tag Affinity Purification—For protein complex analysis of different Cluap1 isoforms HEK293T cells were grown in stable isotope labeling with amino acids in cell culture (SILAC) DMEM (PAA) supplemented with 3 mM l-glutamine (PAA), 10% dialyzed FBS (PAA), 0.55 mM lysine, and 0.4 mM arginine. Light SILAC medium was supplemented with 12C6, 14N2 lysine and 12C6, 14N4 arginine, medium SILAC with 2H4 lysine and 13C6 arginine, and heavy SILAC medium with 13C6, 15N2 lysine, and 13C6, 15N4 arginine. 0.5 mM proline was added to all SILAC

[1] The abbreviations used are: CRISPR/Cas9, clustered regularly interspaced short palindromic repeats/CRISPR-associated nuclease 9; PDGFA, platelet-derived growth factor A; CCDC6, coiled-coil domain-containing protein 6; Cluap1, clusterin-associated protein 1; sgRNA, single guided RNA; IFT, intraflagellar transport; BBS, Bardet–Biedl syndrome; hTERT-RPE-1, human telomerase reverse transcriptase immortalized retina pigmented epithelial cells; HEK293T, human embryonic kidney cells; KO, knockout; TRIP6, thyroid hormone receptor interactor 6; eGFP, (enhanced) green fluorescence protein; EB3, (microtubule plus-) end-binding protein 3; TRAF3IP1, TRAF3-interacting protein 1; MAP4, microtubule-associated protein 4; SILAC, stable isotope labeling with amino acids in cell culture; HPLC, high performance liquid chromatography; TBST, tris-buffered saline with Tween20; DPBS, Dulbecco's Phosphate-Buffered Saline.

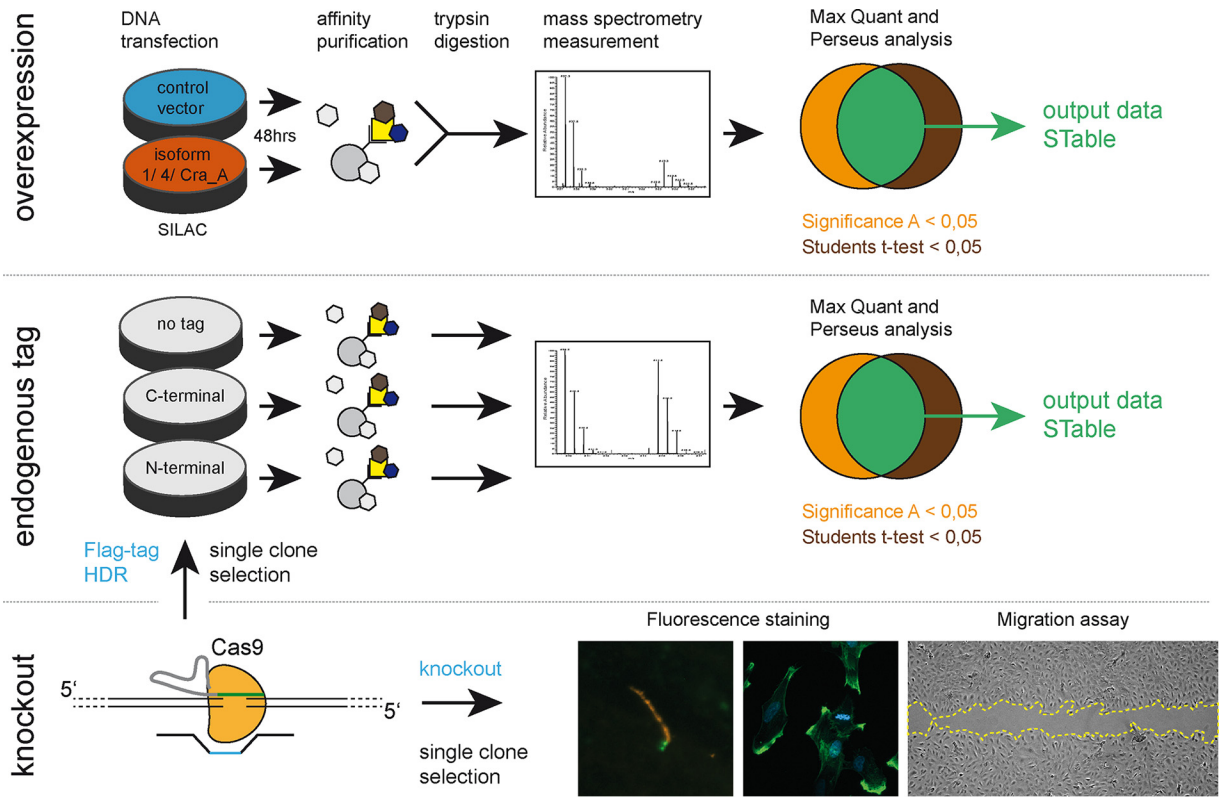

FIG. 1. **Experimental workflow.** For overexpression of Strep/FLAG-tagged Cluap1 isoforms and the empty Strep/FLAG vector as control, SILAC-labeled Hek293T cells were transfected. After 48 h, cells were lysed and Strep affinity purification was performed. The combined eluates (differentially labeled control and isoforms of one experiment, respectively) were trypsin digested and analyzed by mass spectrometry. CRISPR/Cas9-generated endogenously FLAG-tagged Hek293T cells were grown in normal DMEM/10%FBS/2.5% penicillin/streptomycin medium. FLAG affinity purification was followed by trypsin digestion and mass spectrometry. For both, overexpression experiments and endogenously tagged cells, MaxQuant data were statistically analyzed using Perseus (see also "Experimental Design and Statistical Rationale," 31). In parallel, Cluap1 hTERT-RPE1 knockout cells were generated by CRISPR/Cas9 targeting exon 1 and exon 6 for double strand break. Single clones were investigated by fluorescence staining for cilia and cytoskeletal markers and for behavior *e.g.* migration rate.

media to prevent arginine-to-proline conversion. HEK293T were grown in 14-cm plates and transfected with either SF-TAP-empty vector as control or n-terminally SF-TAP-tagged Cluap1 isoforms as described before (27). Endogenously tagged and Cluap1 knockout Hek293T cells were grown in DMEM supplemented with 10% FBS and 0.5% penicillin. After overnight starvation, cells were harvested in 1 ml lysis buffer per plate (0.5% Nonidet-P40, 2% protease inhibitor mixture (Roche), and 1% phosphatase inhibitor cocktails I and II (Sigma-Aldrich) in TBS (30 mM Tris-HCl, pH 7.4, and 150 mM NaCl)). Lysates were rotated 20 min at 35 rpm and 4 °C and centrifuged 10 min at 10,000 *g* and 4 °C. Protein concentration was measured using Bradford reagent and equal amounts of protein per experiment were used. Lysates were incubated with either Strep-Tactin Superflow (IBA) or anti-FLAGM2 agarose beads for 1 h at 4 °C. The resin was washed three times with washing buffer (0.1% Nonidet-P40, 1% phosphatase inhibitor cocktails I and II (Sigma-Aldrich) in TBS) and eluted with strep elution buffer (IBA) or FLAG peptide in TBS, respectively.

Experimental Design and Statistical Rationale—Affinity-purified eluates were precipitated with chloroform and methanol, followed by trypsin digestion as described before (27). LC-MS/MS analysis was performed on Ultimate3000 RSLCnano systems (Thermo Scientific) coupled to either a QExactive Plus or an Orbitrap Fusion Tribrid mass spectrometer (both Thermo Scientific) by a nano spray ion source. Tryptic peptide mixtures were injected automatically and loaded at a flow rate of 30 μl/min in 0.1% trifluoroacetic acid in high performance liquid chromatography (HPLC)-grade water onto a nano trap column (300 μm inner diameter $\times$ 5 mm precolumn, packed with Acclaim PepMap100 C18, 5 μm, 100 Å; Thermo Scientific). After 3 min, peptides were eluted and separated on the analytical column (75 μm inner diameter $\times$ 25 cm, Acclaim PepMap RSLC C18, 2 μm, 100 Å; Thermo Scientific) by a linear gradient from 2% to 30% of buffer B (80% acetonitrile and 0.08% formic acid in HPLC-grade water) in buffer A (2% acetonitrile and 0.1% formic acid in HPLC-grade water) at a flow rate of 300 nl/min over 147 min. Remaining peptides were eluted by a short gradient from 33% or 30% to 95% buffer B in 5 or 10 min. Analysis of the eluted peptides was done on a QExactive Plus or an Orbitrap Fusion Tribrid mass spectrometer. From the high-resolution MS prescan with a mass range of 335 to 1,500, the ten most intense peptide ions were selected for fragment analysis in the Orbitrap depending on intensity (at least 200 counts) and if they were at least doubly charged. The normalized collision energy for higher-energy collisional dissociation was set to a value of 35 or 30 and the resulting fragments were detected with a resolution of 70,000 or 120,000. The lock mass option was activated; the background signal with a mass of 445.12003 was used as lock mass (28). Every ion selected for fragmentation was excluded for 20 or 60 s by dynamic exclusion. MS/MS data were analyzed using the MaxQuant software (version 1.5.3.30) (29, 30). As a digesting enzyme, Trypsin/P was selected with maximal two missed cleavages. Cysteine carbamidom-

ethylation was set for fixed modifications, and oxidation of methionine and N-terminal acetylation was specified as variable modifications. The data were analyzed either by label-free quantification (no fast LFQ, for CRISPR/Cas9-engineered cells) or by triple-labeled (0/0, lysine 4/arginine 6, lysine 8/arginine 10, for overexpression experiments) with the minimum ratio count of 2. The first search peptide tolerance was set to 20, the main search peptide tolerance to 4.5 ppm and the requantify option was selected. For peptide and protein identification, the human subset of the SwissProt database (release 2014_11, #20,194 entries) was used and contaminants were detected using the MaxQuant contaminant search. A minimum peptide number of 1 and a minimum length of seven amino acids were tolerated. Unique and razor peptides were used for quantification. The match between run options was enabled with a match time window of 0.7 min and an alignment time window of 20 min. The statistical analysis was done using the Perseus software (version 1.5.5.3, 31). A minimum of four biological replicates were used for statistics, which represent individual grown and transfected Hek293T dishes. Number of biological replicates (and related controls) were: 5 for endogenously FLAG-tagged Cluap1, 4 for IFT20 overexpression (label-free quantification), 17 for Cluap1 isoform 1, 11 for Cluap1 isoform CRA_a, and 6 for Cluap1 isoform 4 (SILAC labeled). All data were filtered for potential contaminants, peptides only identified by side or reverse sequence. In the groups, minimum half of the samples should have valid values. Mean, standard deviation, and coefficient of variation values of the groups were calculated. Based on the mean value, significance A (Benjamini–Hochberg false discovery rate) was calculated. The stability of protein enrichment within groups was determined using the Student's t test, Only proteins with a significance A < 0.05 and a Student's t test $p < 0.05$ were taken as significantly enriched (Fig. 1, data summarized in Supplemental Table). The mass spectrometry proteomics data have been deposited to the ProteomeXchange Consortium via the PRIDE partner repository with the dataset identifier PXD008343 (https://www.ebi.ac.uk/pride/archive/projects/PXD008343) (32, 33).

Western Blotting—Lysates (20–30 μg) and eluates were boiled at 95 °C for 10 min, separated by SDS-Page and blotted to PVDF membranes (Millipore). After blocking with 5% milk/tris-buffered saline with Tween20 (TBST) solution, membranes were incubated with antibody in 5% milk/TBST. Antibodies used for detection: BBS2 (mouse, Proteintech), IFT88 (goat, Sigma), IFT81 (rabbit, Sigma), IFT27 (rabbit, Proteintech), FLAG®M2-HRP (Sigma), and Cluap1 (rabbit, Proteintech).

Immunofluorescence Staining and Fluorescence Microscopy—HTERT-RPE-1 cells were grown on glass slides and starved for 24–72 h for cilia assembly induction. For rescue experiments and marker gene expression, cells were transfected using lipofectamine 3000. After washing with Dulbecco's phosphate-buffered saline (Dulbecco's Phosphate-Buffered Saline (DPBS), Thermo Scientific), cells were fixed with 4% paraformaldehyde for 10 min at room temperature or 10 min with 100% methanol at −20 °C, permeabilized with 0.3% Triton containing PBS and blocked with 10% normal goat serum, 1% BSA, and 0.1% Tween. Antibodies used for fluorescence imaging: Alexa488 goat anti-mouse/rabbit (Molecular Probes), Alexa568 goat anti-mouse/rabbit (Molecular Probes), acetylated tubulin (mouse, Abcam), rootletin (rabbit, Sigma), tropomyosin (rabbit, Sigma Life Science), and ARL13B (rabbit, Proteintech; mouse, Neuromab). Actin filaments were detected using Atto488-coupled phalloidin (Sigma). For marker gene expression, hTERT-RPE-1 cells were transfected as described above. SfGFP-EB3 and pEGFP-Centrin2 vectors were purchased from Addgene (sfGFP-EB3–7 was a gift from Michael Davidson (Addgene plasmid # 56481); pEGFP-Centrin2 was a gift from Erich Nigg (Addgene plasmid # 41147)).

Fluorescence imaging was done using the Zeiss Imager.Z1 with the ApoTome.2 and the ZEN software. For rescue experiments, the amount of cilia and nuclei of two independent experiments at 5–6 positions per sample were counted, the percentage of ciliated cells were determined, and the p value based on the Students' t test were calculated.

Scratch Assay—HTERT-RPE-1 KO and control cells were grown in six-well plates and starved overnight; the scratch was done using a pipette tip. Subsequently, medium was changed to remove detached and dead cells. Pictures were taken at three different positions per sample, and three biological replicates were analyzed of each control, Cluap1Ex1, or Cluap1Ex6 KO cells. Cell-free area was measured using ImageJ Fiji (34). The significance was calculated based on the Student's t test.

Proliferation Assay—Cells were seeded with a number of 50,000 cells/well in a 12-well plate, fixed for 15 min with DPBS-containing 4% paraformaldehyde, washed two times with water, and incubated with 0.2% crystal violet in 20% ethanol for 20 min at room temperature. After washing three times with water, all samples were air-dried. The stained cells were extracted with 1 ml 10% acetic acid for 20 min at room temperature. The extract absorbance was measured at 590 nm using the Spark® Tecan plate reader. For each time point, three biological replicates were measured, starting with t0 1 day after seeding of the cells.

RESULTS

Protein Complex Analysis of Endogenously Tagged Cluap1—To gain further insight into the molecular function of Cluap1, we aimed at expanding the interactome to identify further, non-IFT proteins. Therefore, we analyzed the interactome on endogenous levels by inserting the FLAG-tag sequence into the genomic Cluap1-coding region to circumvent artificial results caused by overexpression. To cover most of the predicted Cluap1 isoforms, the FLAG-coding sequence was inserted either N-terminally just behind the start codon or C-terminally right before the stop-coding region of exon 12 in HEK293T cells. As repair construct, a single-stranded DNA construct harboring up to 60 bases homology arms and the FLAG-tag-coding sequence was used. A proper sgRNA sequence targeting Cluap1 exon 1 and 12 with no predicted off-targets in other exonic regions than Cluap1 was designed using the online tool CCTop ((35), Supplemental Fig.1*A* and Material and Methods, Table I). For sgRNA cloning and Cas9 expression the pSpCas9(BB)-2A-Puro (PX459) V2.0 vector was used (26). After puromycin treatment (3 μg/ml) and single clone selection, genomic DNA was isolated and screened via PCR for FLAG sequence insertion. The region of interest was amplified and confirmed by Sanger sequencing. For N-terminal FLAG-tag insertion three positive heterozygote (3/31) clones, for C-terminal insertion one homozygote (1/16) clone was identified (Supplemental Figs.1*B* and 1*C*). As a proof of principle, FLAG-Cluap1 clone 10 and Cluap1-FLAG clone 15 were used for FLAG-based purification and analyzed by Western blotting. A Cluap1 and FLAG-positive protein with the size of about 60 kDa was detected for both clones (Fig. 2*B*). We expected to target minimum two Cluap1 isoforms with either N- or C-terminal FLAG insertion based on predicted splice sequences. Surprisingly, with the N-terminal tag

TABLE I
CRISPR/Cas9 constructs and PCR primers

DNA oligos and ssODN Cluap1 constructs were purchased from Integrated DNA Technology (IDT) and Eurofins. For Gateway® cloning of Strep/FLAG-tagged constructs, primers with Gateway®-specific homology arms were used (small letters). The repair (HDR) constructs are shown with FLAG-sequence for tag insertion (bold letters), and exchanged bases (underlined) to avoid sgRNA targeting to the repair construct.

Primer position	Forward 5′–3′	Reverse 5′–3′
5′UTR/intron 1	GGAAGCTTGCAGCCCTCATAG	GGCCAGTGGCAGATAGAGAAC
intron 5/intron 6	TTGCATCAGAGATCCACATGGC	TTTCATTTCCCCACTAACACATCCC
intron11/3′UTR	GACAAGATGTCAGGAATGAGGCA	TGCAAACATAGGAGGCTAAAGCAG
Gateway cloning Cluap isoform 1	aaaaagcaggcttcTCTTTCCGCGACCTCCGC	aagaaagctgggtgttaTCAGAAGTCATTGTCACTCTC
Gateway cloning Cluap CRA_a	aaaaagcaggcttcTCTTTCCGCGACCTCCGC	aagaaagctgggtgttaTCAGCCACTCCCATCTATG
sgRNA	**sgRNA Top**	**sgRNA Bottom**
Exon1 sgRNA	CACCGCTGCCTTACTGCGGAGGTCG	AAACCGACCTCCGCAGTAAGGCAGC
Exon 6 sgRNA	CACCGCTCGTTTATTTCCAGAGGTC	AAACGACCTCTGGAAATAAACGAGC
Exon 12 sgRNA	CACCGTCATTGTCACTCTCATCCAG	AAACCTGGATGAGAGTGACAATGAC
HDR construct FLAG N-term	GCGAGCAGTTGCGACCCTGGGCTCCTGGGGACCTGAGCGTTATG**GATTATAAAGATGATGATGATAAA**TC TTTTCGCGACCTTCGCAGTAAGGCAGCCCCGCGCCCCTGTGACCTGCGGG	
HDR construct FLAG C-term	TCGAAGGGTCCGGAAATCTGAACCCCTTGATGAAAGTGACAATGACTTC**GATTATAAAGATGATGATGAT AAA**TGACCCTTTTGCCAAGGGACCCTGGCAGATTAAAACCCTCAGACTTG	

only, a second Cluap1 isoform was purified that could be due to an isoform specific expression level in this cell line.

To analyze the Cluap1 protein interaction, we performed FLAG affinity purification of the endogenous FLAG-tagged clones and CRISPR/Cas9 HEK298T control cells and investigated protein complex formation by quantitative mass spectrometry. The label-free quantification and the identification of five biological replicates was done using the MaxQuant software and statistics was calculated using Perseus (29, 31). Proteins, which were enriched with a significance A $<$ 0.05 and a Student's *t* test $p < 0.05$ in the FLAG-Cluap1 samples compared with the control were considered as interactors (Fig. 2*A*, Supplemental Table). The whole IFT-B complex was nicely accumulated in Cluap1 eluates. Besides these already-described IFT proteins, new interactors with some appearing in N-terminal as well as C-terminal Cluap1-tagged cells but also distinguishable complex components were detected. In both cell lines, the new Cluap1 complex member Septin-10 and the BBSome protein BBS2 were enriched, whereas BBS2 could be identified by Western blotting only (Fig. 2*B*). In eluates of N-terminal tagged cells regulators of the cytoskeleton were found (*e.g.* Ephrin-B1, TRIP6, Fascin, TBCD) that indicated a role of Cluap1 in cytoskeletal arrangement (Figs. 2*A* and 2*B*, Supplemental Table).

Cluap1 Complexes Assemble in an Isoform-specific Manner—Next, to investigate how the dataset gained by endogenously tagged protein correlates with overexpression data of different isoforms and to detect isoform-specific interactomes, we used the SILAC-labeling approach and ectopic expression of three different Cluap1 isoforms.

The short isoform 4 lacking the N-terminal IFT-B binding domain, the isoform CRA_a encoding an alternative spliced C-term and the well-described isoform 1 were Strep/FLAG (SF-TAP) -tagged as described before (ENST00000571025.5, ENST00000572600.5, ENST00000341633.9, (17, 36)). Differentially supplemental table isotope-labeled HEK293T cells were transfected either with the empty control vector or the SF-TAP-Cluap1 isoforms; protein complexes were purified and analyzed by mass spectrometry as described before (36). As expected, IFT-B proteins were co-purified with isoform 1 and CRA_a, whereas with isoform 4 only IFT20 was identified. Interestingly, BBS7 interaction was detected with both the short isoform 4 and the long variant 1, indicating a central role of Cluap1 in IFT-B-BBSome complex association (Fig. 2*C*, Supplemental Fig. 2*A*, Supplemental Table). The fact that both isoforms show an interaction with BBS proteins is potentially due to dimerization of Cluap1 isoforms (17). Anyhow, there was no evidence for cytoskeleton-influencing proteins as it was seen for endogenously tagged Cluap1 purification. Nevertheless, due to the artificial overexpression, some functional relevant proteins may be hidden in these experiments, underlining the importance of studies comparing protein complex analysis on the endogenous level *versus* overexpression experiments. To investigate if Cluap1 has a role in cytoskeletal arrangement, CRISPR/Cas9-mediated KO cell lines were generated.

CRISPR/Cas9-mediated Cluap1 Knockout Disturbs IFT20 Complex and Cilia Assembly—Cluap1 is one of the IFT-B proteins necessary for ciliary assembly. KO of such an essential protein leads to embryonic lethality, which makes detailed functional analysis difficult (19, 20). Here, hTERT-RPE-1 and HEK293T cells were used for targeted Cluap1 KO followed by protein complex and "phenotypic" analysis. A Cluap1 exon 1 and exon 6 targeting sgRNA sequence was determined and cloned into the pSpCas9(BB)-2A-Puro (PX459) V2.0 vector as described before (26). Single clones with a premature stop codon, and no detectable full-length protein expression were selected for further analysis (Supplemental Fig. 3*A*). As a

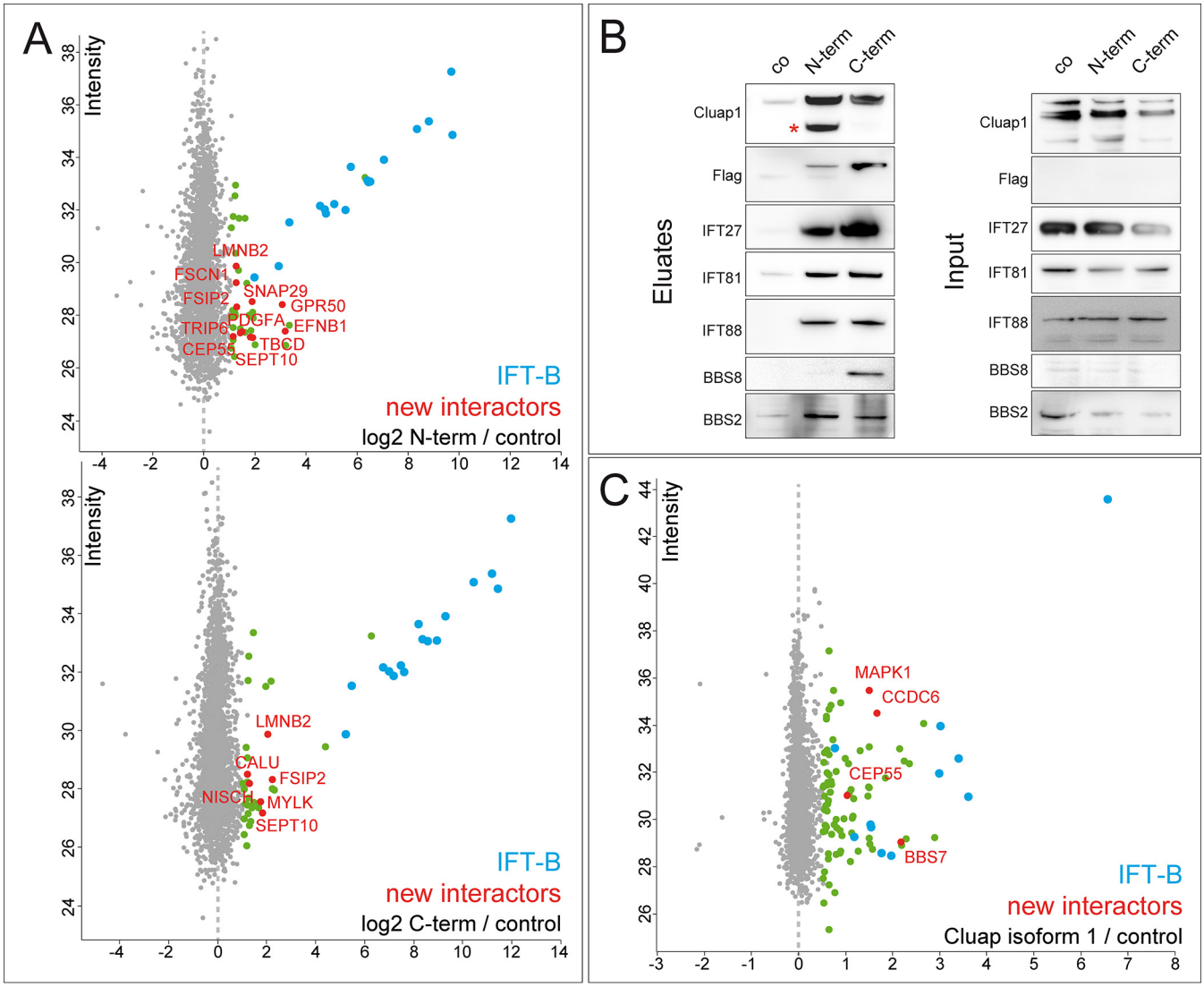

FIG. 2. **Protein complex analysis using endogenously tagged Cluap1.** (*A*) The mass spectrometry data of five biological replicates were statistically analyzed using MaxQuant and Perseus (highlighted: proteins with significance A $<$ 0.05 and student's *t* test $p < 0.05$). The whole IFT-B complex could be detected in both, C- and N-terminally tagged Cluap1 HEK293T cells (blue). (*B*) Mass spectrometry data were validated by Western blotting. Using a Cluap1 antibody, two isoforms were detected in N- but only one in C-terminally tagged cells. (*C*) The SILAC-labeling approach was used to investigate protein complex formation of single Cluap1 isoforms. With overexpression of the isoform 1 some IFT-B proteins, the BBSome component BBS7 and new factors, *e.g.* CCDC6 and CEP55, were enriched (17 biological replicates, highlighted: proteins with significance A $<$ 0.05 and student's *t* test $p < 0.05$).

proof of principle, we used HEK293T Cluap1Ex1 KO cells for IFT20 protein complex analysis. In control cells, IFT20 bound to the IFT-B complex components Cluap1, IFT172, IFT57, IFT80, and IFT54/TRAF3IP1. In Cluap1Ex1 KO cells, the IFT20 interaction with all IFT-B proteins except IFT54/TRAF3IP1 was lost due to loss of Cluap1 expression (Supplemental Fig. 3*B*). These results indicated that Cluap1 could be the linking protein between IFT20/TRAF3IP1 and the IFT-B2 subcomplex, which is in line with data published by Michael Taschner and his colleagues (18). Because HEK293T cells are small and do not display robust ciliation, cytoskeletal arrangement, and polarization, the phenotypic analysis was performed in the retinal hTERT-RPE-1 cell line.

HTERT-RPE-1 control cells were grown under starving condition to induce cilia assembly. About 60% of control cells displayed cilia after 24 h. In contrast, in Cluap1Ex1 and Ex6 KO cells, no cilia were detected. This ciliary phenotype was rescued by re-expression of the IFT-B complex binding Cluap1 isoform 1, which was a proof for the specificity of the CRISPR/Cas9-mediated Cluap1 KO excluding off-target effects as reason for absence of cilia (Fig. 3) (17, 18).

Actin Cytoskeleton Arrangement and Migration Is Affected by Cluap1 Knockout—In the interactome study of endogenously tagged Cluap1, new complex components have been identified, which are described to be modulators of the cytoskeleton arrangement. To analyze the function of Cluap1 for

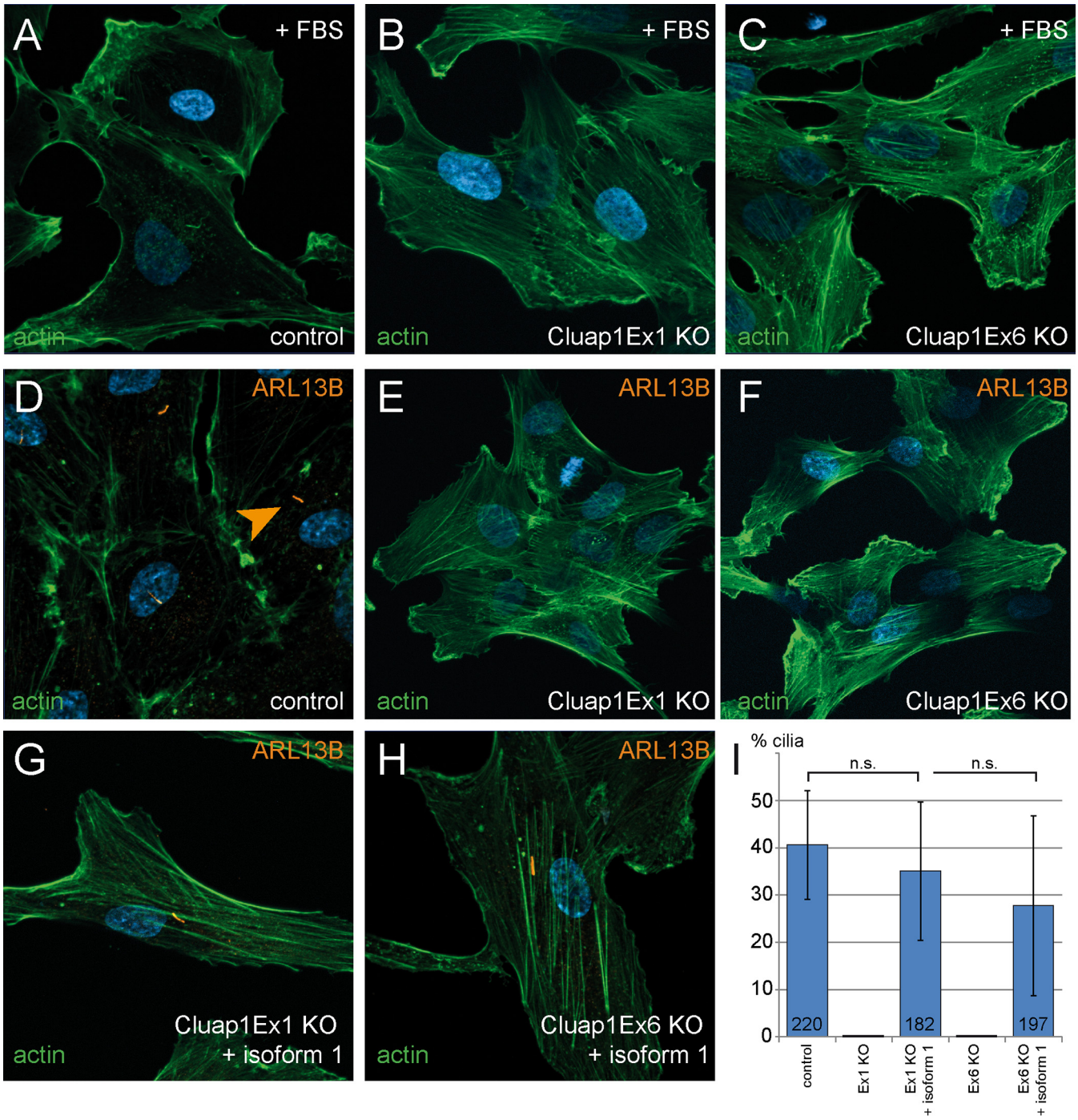

FIG. 3. **No cilia and an increase of actin filaments in Cluap1 Ex1 and Ex6 KO.** The cell phenotype was observed either under complete (+FBS, *A–C*) or starving condition (-FBS, *D–H*). Cilia were stained with ARL13B (red), and actin was visualized in green using Phalloidin-Alexa488 (*A–H*). Cilia were absent in Cluap1Ex1 KO and Ex6 KO hTERT-RPE-1 cells (*E*, *F*) whereas control cells showed normal cilia assembly after 24 h of starvation (*D*). Phalloidin-Alexa488 staining revealed a high amount of filamentous actin in KO (*B*, *C*, *E*, *F*) compared with control cells (*A*, *D*). Ectopic expression of the IFT-B complex binding Cluap1 isoform 1 could rescue the ciliary assembly but not the actin organization (*G–I*) (*I*) Nuclei and cilia of two independent experiments at 5–7 positions per sample were counted, and the percentage of ciliated cells was calculated. The total number of counted cells is shown at the bottom of each bar. No cilia were detected in both KO cell lines.

cilia-independent processes in more detail, proliferation, cytoskeletal arrangement and migration was investigated in Cluap1 KO cell lines. To exclude alterations in cell cycle regulation, proliferation was analyzed using the crystal violet assay. No difference between control and KO cells was seen (Fig. 4*E*). Acetylated tubulin staining and overexpression of

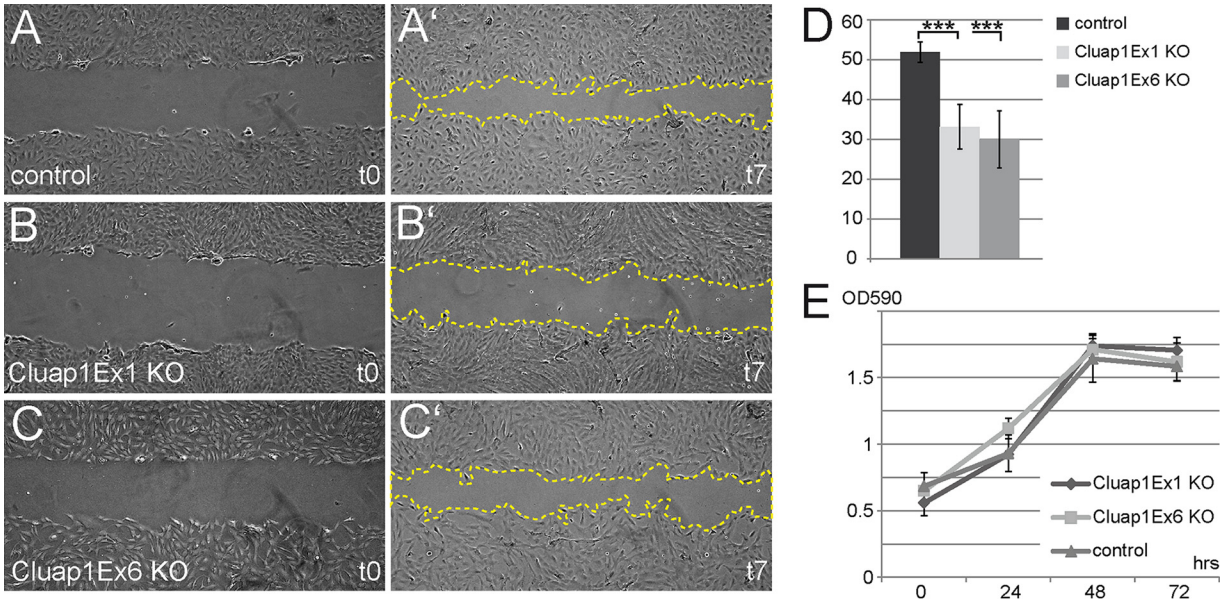

FIG. 4. **Migration was slowed down in Cluap1Ex1 and Ex6 KO cells.** (*A–C*) Control and KO sells were incubated in starvation medium for 24 h prior to scratch. Images of two independent experiments with three biological replicates at three positions each were captured after scratch (t0, *A–C*) and 7 h later (t7, *A′–C′*). (*D*) The cell-free area was measured using ImageJ Fiji and the percentage of closure was calculated. The significance was calculated using the Student's *t* test. (*E*) The proliferation rate was measured using the crystal violet assay. There was no significant difference in cell number at any time point between control and KO cells.

EGFP-EB3 revealed no change in the microtubule arrangement in hTERT-RPE-1 KO cells compared with CRISPR/Cas9 control cells (Supplemental Fig. 4). Also the basal body positioning in relation to the nucleus, as investigated by rootletin staining and EGFP-Centrin2 overexpression, as well as intermediate filament arrangement stained with Vimentin, were normal (Supplemental Fig. 4). Interestingly, when Alexa488-coupled phalloidin for visualization of actin was used, an alteration in actin organization with more evenly oriented filamentous structures in KO cells compared with control cells was detected (Fig. 3). Re-expression of the three Cluap1 isoforms used in this study, either alone or in combination, did not rescue the actin phenotype. One explanation could be that the actin rearrangement is caused by an off-target effect of the sgRNAs used for generation of Cluap1 KO cell lines. This seems to be unlikely because the same phenotype was seen in cell lines generated by using two different sgRNA sequences targeting different exonic regions of Cluap1. In addition, some Cluap1 complex components were regulators of the actin cytoskeleton suggesting a Cluap1-dependent modulation of actin arrangement. Another explanation would be that the actin cytoskeleton is not regulated by an on–off signal but by the balanced expression and localization of different Cluap1 isoforms.

Because the actin cytoskeleton dynamics are substantial for cellular migration, the migration rate was investigated using the scratch assay. The cell-free area was measured using ImageJ Fiji, and the percentage of closure was calculated. The Cluap1Ex1 and Ex6 KO cell migration was highly significantly slower compared with control cells (control 52% gap closure ±2.5, Cluap1Ex1 KO 33% ± 5.7, Cluap1Ex6 KO 30% ± 7.2; Fig. 4).

Taken together, our results imply that the IFT-B protein Cluap1 is involved, in a complex and isoform specific manner in actin cytoskeleton regulation and actin-related processes like migration behavior of cells.

DISCUSSION

In this study, we used the CRISPR/Cas9-mediated tagging of Cluap1, which enables a proteomic complex analysis on the endogenous expression level, erasing artifacts due to ectopic expression. We decided to use the FLAG-tag sequence without any linker or selection cassette to minimize the risk of getting changes in protein folding due to insertion of huge DNA elements (24, 25). With N- and C-terminal tag insertion, the 60kDa Cluap1 protein could be purified. Interestingly, only with the N-terminal tag a second FLAG-negative isoform was seen. Cluap1 is described to dimerize via its coiled-coil domain (AA120–328) without the very C-terminal region, but potentially protein folding could be influenced negatively by the FLAG-tag, regulating dimerization with other isoforms (17). Nevertheless, the whole IFT-B complex was nicely purified with each tagged Cluap1 version. The Cluap1 interactome included structural relevant proteins such as Ephrin-B1, Fascin, and TBCD, hinting toward a role of Cluap1 in cytoskeletal arrangement. Interestingly, Cluap1 seemed to interact with signaling pathway components such as PDGFA and TRIP6, which suggest a role in signal transduction, as well.

Besides the analysis of endogenous Cluap1 protein complexes, overexpression of three different isoforms was performed to compare protein complex assembly. As described before, the short isoform 4 did not interact with IFT-B complex components except IFT20 (17). Surprisingly, proteins of the BBSome, BBS2, and BBS7 were found to be part of the Cluap1 isoform 1 and 4 complex. As for endogenously tagged cells, BBS2 enrichment was only detected by Western blot analysis. In addition, CCDC6, a protein involved in cancer development and cell cycle regulation, stably interacted with all three Cluap1 isoforms (37). In line with this, MAPK1 was enriched in Cluap1 eluates, hinting at a role in cell cycle regulation.

Endogenous analysis using genome-edited cells is suitable, but also here, there might be issues with the tag. Therefore, tagging both termini is advisable. Even though overexpression can lead to artifacts and the risk for false positives or false negatives is relatively high, these approaches can be advantageous (3). Comparing isoforms for example is in most cases not achievable with endogenous tags or antibodies. In addition, we could detect interactors only by this approach but not in endogenous precipitations. Even though this could simply be a matter of sensitivity, it shows that ectopic expression can give quick and meaningful results with a higher risk of false positive detections, though.

Based on the proteomic data, we hypothesized that Cluap1 has a function cytoskeletal arrangement. We generated two different Cluap1 KO cell lines, which, as expected, showed cilia assembly defects. Interestingly, both cell lines displayed an increased filamentous actin organization compared with the control. In line with that, the migration was slowed down in KO cells, which is most likely due to the static actin filaments (38, 39). We were able to rescue the cilia assembly by re-expression of the long IFT-B complex-binding and coiled-coil domain-containing Cluap1 isoform 1 but not with the N-terminal truncated isoform 4. We did not succeed to rescue the actin arrangement, neither by re-expression of three different Cluap1 isoforms separately nor by co-expression of the latter. Because we used two different sgRNAs targeting different exonic regions, an off-target effect is unlikely. The failure to rescue this phenotype might be due to an imbalance between the different Cluap1 isoforms or because a yet unknown isoform might be necessary for this function. Interestingly, actin cytoskeleton modulating functions are described for other ciliary proteins, as well. In hypomorphic IFT88 (orpk) cells, the actin filamentous structure was increased and cortical F-actin expression was altered (40). The deletion of IFT80 results in increased actin stress fiber numbers and disrupted cilia formation, which could be partially rescued by Cytochalasin D treatment (41). Conversely, loss of function of the actin-depolymerizing factors NudC and cofilin-1 promotes cilia assembly (42). But Cluap1 may not only modulate the actin organization by binding to structural components like Fascin and Ephrin-B1 but also by its interactions with TRIP6, which is suggested to be an actin and migration-modulating factor (43, 44). In contrast to Cluap1 loss of function, siRNA mediated knockdown of TRIP6 resulted in increased invasiveness of cells accompanied by increased filamentous actin (44). In line with that, we suggest that the alterations of the actin cytoskeleton are not due to the lack of cilia but rather to an alternative function of Cluap1. This might also be true for other IFT proteins.

Based on the data provided by this study, a complex and isoform-specific function of the IFT-B member Cluap1 for cilia as well as for basic cellular events like cytoskeletal arrangement was described. Anyhow, the hierarchy between cilia-dependent and independent signaling influencing the actin cytoskeleton or vice versa could not be elucidated, but the dataset gained by the comprehensive complex analysis provides the perfect basis for further investigation.

Acknowledgments—We thank Prof. Ronald Roepman for sharing the Cluap1 isoform 4 construct and his group for the discussion of the project.

DATA AVAILABILITY

The mass spectrometry proteomics data have been deposited to the ProteomeXchange Consortium via the PRIDE partner repository with the dataset identifier PXD008343 (https://www.ebi.ac.uk/pride/archive/projects/PXD008343; 32, 33).

* The research leading to these results received funding from the Clinical Faculty of Tuebingen fortuene program.

S This article contains supplemental material.

¶ These authors contributed equally to this work.

To whom correspondence should be addressed: E-mail: Tina.Beyer@uni-tuebingen.de or karsten.boldt@uni-tuebingen.de.

Author contributions: T.B., M.U., and K.B. designed research; T.B., S.B., K.J., N.H., M.M., and Y.W. performed research; T.B. and K.B. analyzed data; and T.B., M.U., and K.B. wrote the paper.

REFERENCES

1. Cong, L., Ran, F. A., Cox, D., Lin, S., Barretto, R., Habib, N., Hsu, P. D., Wu, X., Jiang, W., Marraffini, L. A., and Zhang, F. (2013) Multiplex genome engineering using CRISPR/VCas systems. *Science* **339,** 819–823
2. Mali, P., Yang, L., Esvelt, K. M., Aach, J., Guell, M., DiCarlo, J. E., Norville, J. E., and Church, G. M. (2013) RNA-guided human genome engineering via Cas9 prashant. *Science* **339,** 823–826
3. Gibson, T. J., Seiler, M., and Veitia, R. A. (2013) The transience of transient overexpression. *Nat. Methods* **10,** 715–721
4. Spassky, N., and Meunier, A. (2017) The development and functions of multiciliated epithelia. *Nat. Rev. Mol. Cell Biol.* **18,** 423–436
5. Spasic, M., and Jacobs, C. R. (2017) Primary cilia: Cell and molecular mechanosensors directing whole tissue function. *Semin. Cell Dev. Biol.* **71,** 42–52
6. May-Simera, H., Nagel-Wolfrum, K., and Wolfrum, U. (2017) Cilia—The sensory antennae in the eye. *Prog. Retin. Eye Res.* **60,** 144–180
7. Goetz, S. C., and Anderson, K. V. (2010) The primary cilium: A signaling center during vertebrate development. *Nat. Rev. Genet*. **11,** 331–344
8. Fliegauf, M., Benzing, T., and Omran, H. (2007) When cilia go bad: Cilia defects and ciliopathies. *Nat. Rev. Mol. Cell Biol.* **8,** 880–893
9. Lechtreck, K. F., Van De Weghe, J. C., Harris, J. A., and Liu, P. (2017) Protein transport in growing and steady-state cilia. *Traffic* **18,** 277–286
10. Verhey, K. J., Dishinger, J., and Kee, H. L. (2013) Kinesin motors and primary cilia. *Biochem. Soc. Trans.* **80,** 631–637
11. Lechtreck, K. F. (2015) IFT-cargo interactions and protein transport in cilia. *Trends Biochem. Sci.* **40,** 765–778

12. Galgano, D., Onnis, A., Pappalardo, E., Galvagni, F., Acuto, O., and Baldari, C. T. (2017) The T cell IFT20 interactome reveals new players in immune synapse assembly. *J. Cell Sci.* **130**, 1110–1121
13. Bizet, A. A., Becker-Heck, A., Ryan, R., Weber, K., Filhol, E., Krug, P., Halbritter, J., Delous, M., Lasbennes, M.-C., Linghu, B., Oakeley, E. J., Zarhrate, M., Nitschké, P., Garfa-Traore, M., Serluca, F., Yang, F., Bouwmeester, T., Pinson, L., Cassuto, E., Dubot, P., Elshakhs, N. A., Sahel, J. A., Salomon, R., Drummond, I. A., Gubler, M.-C., Antignac, C., Chibout, S., Szustakowski, J. D., Hildebrandt, F., Lorentzen, E., Sailer, A. W., Benmerah, A., Saint-Mezard, P., and Saunier, S. (2015) Mutations in TRAF3IP1/IFT54 reveal a new role for IFT proteins in microtubule stabilization. *Nat. Commun.* **6,** 8666
14. Delaval, B., Bright, A., Lawson, N. D., and Doxsey, S. (2011) The cilia protein IFT88 is required for spindle orientation in mitosis. *Nature Cell Biol.* **13,** 461–468
15. Boehlke, C., Janusch, H., Hamann, C., Powelske, C., Mergen, M., Herbst, H., Kotsis, F., Nitschke, R., and Kuehn, E. W. (2015) A cilia independent role of Ift88/polaris during cell migration. *PLoS ONE* **10,** e0140378
16. Borovina, A., and Ciruna, B. (2013) IFT88 Plays a cilia- and PCP-independent role in controlling oriented cell divisions during vertebrate embryonic development. *Cell Rep.* **5,** 37–43
17. Katoh, Y., Terada, M., Nishijima, Y., Takei, R., Nozaki, S., Hamada, H., and Nakayama, K. (2016) Overall architecture of the intraflagellar transport (IFT)-B complex containing cluap1/IFT38 as an essential component of the IFT-B peripheral subcomplex. *J. Biol. Chem.* **291,** 10962–10975
18. Taschner, M., Weber, K., Mourão, A., Vetter, M., Awasthi, M., Stiegler, M., Bhogaraju, S., and Lorentzen, E. (2016) Intraflagellar transport proteins 172, 80, 57, 54, 38, and 20 form a supplemental table tubulin-binding IFT-B2 complex. *EMBO J.* **35,** 773–790
19. Pasek, R. C., Berbari, N. F., Lewis, W. R., Kesterson, R. A., and Yoder, B. K. (2012) Mammalian clusterin-associated protein 1 is an evolutionarily conserved protein required for ciliogenesis. *Cilia* **1,** 20
20. Botilde, Y., Yoshiba, S., Shinohara, K., Hasegawa, T., Nishimura, H., Shiratori, H., and Hamada, H. (2013) Cluap1 localizes preferentially to the base and tip of cilia and is required for ciliogenesis in the mouse embryo. *Dev. Biol.* **381,** 203–12
21. Lee, C., Wallingford, J. B., and Gross, J. M. (2014) Cluap1 is essential for ciliogenesis and photoreceptor maintenance in the vertebrate eye. *Investigat. Ophthalmol. Visual Sci.* **55,** 4585–4592
22. Soens, Z. T., Li, Y., Zhao, L., Eblimit, A., Dharmat, R., Li, Y., Chen, Y., Naqeeb, M., Fajardo, N., Lopez, I., Sun, Z., Koenekoop, R. K., and Chen, R. (2016) Hypomorphic mutations identified in candidate Leber congenital amaurosis disease gene CLUAP1. *Genet. Med.* **18,** 1044–1051
23. Takahashi, M., Lin, Y.-M., Nakamura, Y., and Furukawa, Y. (2004) Isolation and characterization of a novel gene CLUAP1 whose expression is frequently upregulated in colon cancer. *Oncogene* **23,** 9289–9294
24. Dalvai, M., Loehr, J., Jacquet, K., Huard, C. C., Roques, C., Herst, P., Côté, J., and Doyon, Y. (2015) A scalable genome-editing-based approach for mapping multiprotein complexes in human cells. *Cell Rep.* **13,** 621–633
25. Baillat, D., Russell, W. K., and Wagner, E. J. (2016) CRISPR-Cas9 mediated genetic engineering for the purification of the endogenous integrator complex from mammalian cells. *Protein Expr. Purif.* **128,** 101–108
26. Ran, F. A., Hsu, P. D., Wright, J., Agarwala, V., Scott, D. A., and Zhang, F. (2013) Genome engineering using the CRISPR-Cas9 system. *Nat. Protoc.* **8,** 2281–2308
27. Gloeckner, C. J., Boldt, K., and Ueffing, M. (2009) Strep/FLAG tandem affinity purification (SF-TAP) to study protein interactions. *Curr. Protocols Protein Sci.* **57,** 19.20.1–19.20.19
28. Olsen, J. V., de Godoy, L. M., Li, G., Macek, B., Mortensen, P., Pesch, R., Makarov, A., Lange, O., Horning, S., and Mann, M. (2005) Parts per million mass accuracy on an Orbitrap mass spectrometer via lock mass injection into a C-trap. *Mol. Cell. Proteomics* **4,** 2010–2021
29. Cox, J., and Mann, M. (2008) MaxQuant enables high peptide identification rates, individualized p.p.b.-range mass accuracies and proteome-wide protein quantification. *Nat. Biotechnol.* **26,** 1367–1372
30. Cox, J., Matic, I., Hilger, M., Nagaraj, N., Selbach, M., Olsen, J. V., and Mann, M. (2009) A practical guide to the MaxQuant computational platform for SILAC-based quantitative proteomics. *Nat. Protoc.* **4,** 698–705
31. Tyanova, S., Temu, T., Sinitcyn, P., Carlson, A., Hein, M. Y., Geiger, T., Mann, M., and Cox, J. (2016) The Perseus computational platform for comprehensive analysis of (prote) omics data. *Nat. Methods* **13,** 731–740
32. Tardif, S. D., Aagaard, K. M., Archidiacono, N., Rayan, N. A., Batzer, M. A., Dao, M. D., Jong, P. J. De, Rosario, R. C., Delehaunty, K. D., Dinh, H. H., Eichler, E., Fitzgerald, S., Flicek, P., Fontenot, C. C., Fowler, R. G., Fronick, C., Lucinda, A., Fulton, R. S., Gabisi, R. A., Gerlach, D., Graves, T. A., and Gunaratne, P. H. (2015) ProteomeXchange provides globally co-ordinated proteomics data submission and dissemination. *Nat. Biotechnol.* **46,** 850–857
33. Vizcaíno, J. A., Csordas, A., del-Toro, N., Dianes, J. A., Griss, J., Lavidas, I., Mayer, G., Perez-Riverol, Y., Reisinger, F., Ternent, T., Xu, Q. W., Wang, R., and Hermjakob, H. (2016) 2016 update of the PRIDE database and its related tools. *Nucleic Acids Res.* **44,** D447–D456
34. Schindelin, J., Arganda-Carreras, I., Frise, E., Kaynig, V., Longair, M., Pietzsch, T., Preibisch, S., Rueden, C., Saalfeld, S., Schmid, B., Tinevez, J.-Y., White, D. J., Hartenstein, V., Eliceiri, K., Tomancak, P., and Cardona, A. (2012) Fiji: An open source platform for biological image analysis. *Nat. Methods* **9**, 676–682
35. Stemmer, M., Thumberger, T., del Sol Keyer, M., Wittbrodt, J., and Mateo, J. L. (2015) CCTop: An intuitive, flexible and reliable CRISPR/Cas9 target prediction tool. *PLoS ONE* **10**, e0124633
36. Boldt, K., Gloeckner, C. J., Texier, Y., von Zweydorf, F., and Ueffing, M. (2014) *supplemental table Isotope Labeling by Amino Acids in Cell Culture (SILAC): Methods and Protocols*, B. Warscheid, ed. New York: Springer, 177–190
37. Leone, V., Mansueto, G., Pierantoni, G. M., Tornincasa, M., Merolla, F., Cerrato, A., Santoro, M., Grieco, M., Scaloni, A., Celetti, A., and Fusco, A. (2010) CCDC6 represses CREB1 activity by recruiting histone deacetylase 1 and protein phosphatase 1. *Oncogene* **29,** 4341–4351
38. Inagaki, N., and Katsuno, H. (2017) Actin waves: Origin of cell polarization and migration? *Trends Cell Biol.* **27,** 515–526
39. Callan-Jones, A. C., and Voituriez, R. (2016) Actin flows in cell migration: From locomotion and polarity to trajectories. *Curr. Opin. Cell Biol.* **38,** 12–17
40. Wang, Z., Wann, A. K., Thompson, C. L., Hassen, A., Wang, W., and Knight, M. M. (2016) IFT88 influences chondrocyte actin organization and biomechanics. *Osteoarthr. Cartil.* **24,** 544–554
41. Yuan, X., Cao, J., He, X., Serra, R., Qu, J., Cao, X., and Yang, S. (2016) Ciliary IFT80 balances canonical versus non-canonical hedgehog signalling for osteoblast differentiation. *Nat. Commun.* **7,** 11024
42. Zhang, C., Zhang, W., Lu, Y., Yan, X., Yan, X., Zhu, X., Liu, W., Yang, Y., and Zhou, T. (2016) NudC regulates actin dynamics and ciliogenesis by stabilizing cofilin 1. *Cell Res.* **26,** 239–253
43. Lin, V. T., and Lin, F. T. (2011) TRIP6: An adaptor protein that regulates cell motility, antiapoptotic signaling and transcriptional activity. *Cell Signal.* **23,** 1691–1697
44. Guryanova, O. A., Sablina, A. A., Chumakov, P. M., and Frolova1, E. I. (2005) Downregulation of TRIP6 gene expression induces actin cytoskeleton rearrangements in human carcinoma cell lines O. *Mol. Biol.* **39,** 905–909